DOI: 10.47355/aset.v4i2.65

J. ASET

Numerical Simulation of Single Droplet Phenomenon to Investigate Density Field Characteristics Using Finite Volume-Front Tracking Method

Dondi Kurniawan 1*, Angga Darma Prabowo 1,

- ¹ Department of Mechanical Engineering, Faculty of Engineering, Universitas Lampung, Gedung H Lt. 2, Jl. Prof. Soemnantri Brojonegoro No. 1, Bandar Lampung 35143, Indonesia
- * Correspondence: dondikur17@eng.unila.ac.id

Received: 24.9.2024; Accepted: 05.11.2024; Published: 31.12.2024

Abstract: Modeling the phenomenon of a single droplet impacting a horizontal solid surface is carried out using the finite volume - front tracking method. This work aims to study the characteristics of droplets, especially the density field. The interface is tracked using the front-tracking method based on the location of the density jump. The governing equations used in this modeling are the 2D continuity and Navier-stokes equations for the unsteady and incompressible cases. The validation of this research is done by comparing the results obtained using the implicit scheme with the results developed by Tryggvason 2012 using the explicit scheme. This research shows that surface tension plays an important role in the shape of the droplet when moving and impacting the surface. In addition, the grid size is known to have an influence on this modeling. The smaller the grid size (the more the number of grids), the more accurate the density jump obtained and closer to the exact results. This research is expected to provide a deeper understanding of microscopic phenomena, especially the droplet phenomenon.

Keywords: Numerical Simulation, Front-tracking, Droplet

1. Introduction

Work on single droplets has great significance in understanding various physical and chemical phenomena that occur in liquid-based systems, such as internal combustion and liquid sprays. In combustion engines, fuel droplets perform an important role in determining the efficiency, emissions, and stability of the combustion process. Single-droplet modeling has become a useful tool for predicting evaporation and combustion behavior, thus supporting the development of more efficient system designs [1][2].

In the applications of liquid spray, such as irrigation and medical nebulizers, droplet parameters such as size and velocity greatly affect efficiency and precision levels. A fluorescence-based technique was recently introduced to measure the temperature of droplets in sprays, which helps provide deeper insights into the heat and mass transfer process [3].

Single-droplet research has also played an important role in the development of advanced combustion systems, such as jet engines. Studies show that fuel atomization and its interaction with the surrounding air turbulence have a significant impact on the fuel vaporization and mixing process, which contributes to improved efficiency as well as reduced pollutant emissions[4]. In printing

technologies such as inkjet printing, precise control of droplet size and shape is a key success factor. Research related to atomization and droplet distribution has provided valuable insights to produce high quality prints[5],[6],[7].

In modern liquid-based refrigeration systems, the interaction of liquid droplets with hot surfaces plays an important role in determining the effectiveness of heat transfer. The study of single droplets provides essential data regarding evaporation rates and phase transitions, which form the basis for the development of high-performance refrigeration systems[8].

Related research on the droplet phenomenon was conducted by [9] using the finite volume method and [10] using the finite difference method. Both studies were conducted with a front-tracking scheme to track the movement of the interface between the two liquid phases and the surrounding fluid. It is obtained from previous studies that the value of density and gravitational force greatly affects the spreading ratio [11].

As a whole, single-droplet research provides an in-depth understanding of microscopic phenomena that directly affect system performance at the macroscopic scale. With the support of cutting-edge technologies such as high-resolution imaging and numerical simulation, these studies are increasingly relevant for fostering innovation in the fields of green energy and precision manufacturing [12].

2. Mathematical Modeling and Governing Equations

Multiphase flow is a complex phenomenon involving at least two or more fluids. In this research, the interfacial diffusion approach involves two fluids, the droplet and the surrounding fluid where the dynamics and behavior of the interface changes are influenced by surface tension. In addition, other variables that also contribute significantly to the properties of a fluid are density, viscosity, and the influence of surface tension and contact angle [10], [13], [14]. The involvement of these variables is written in a governing equation to be able to describe the phenomena that occur in a case. The governing equation that describes the movement of both liquid and gaseous fluids is the Navier-Stokes equation. In simplifying this concept, the equations used are the continuity and Navier-Stokes equations for incompressible and unsteady flow cases [9],[10].

2.1. Governing Equations

In this present study, the governing equations used are the equations of continuity and Navier-Stokes. The equations used for the case of incompressible unchanging flow and two-dimensional unsteady flow, so the governing equations are presented as follows,

$$\frac{\partial \rho}{\partial t} + \rho \left(\frac{\partial u}{\partial x} + \frac{\partial v}{\partial y} \right) = 0 \tag{1}$$

$$\frac{\partial \rho}{\partial t} + u \frac{\partial u}{\partial x} + v \frac{\partial u}{\partial y} = \frac{1}{\rho} \frac{\partial p}{\partial x} + v \left(\frac{\partial^2 u}{\partial x^2} + \frac{\partial^2 u}{\partial y^2} \right) + g_x + f \tag{2}$$

$$\frac{\partial \rho}{\partial t} + u \frac{\partial v}{\partial x} + v \frac{\partial v}{\partial y} = \frac{1}{\rho} \frac{\partial p}{\partial x} + v \left(\frac{\partial^2 v}{\partial x^2} + \frac{\partial^2 v}{\partial y^2} \right) + g_y + f \tag{3}$$

Where, u and v denote the velocity in the x and y axis directions, p denotes the pressure value, ρ is the density and v is the viscosity value.

2.2. Governing Equations

Discretization of the governing equation is conducted implicitly with the fractional-step method. This method is one way the momentum equation becomes implicit by means of 2 discretization steps,

namely by partially deriving the x component first and then solving the derivative part of the y component with the Thomas algorithm[9], [10], [15].

$$\frac{\partial u}{\partial t} = -\frac{\partial}{\partial x} \left(u^2 \right) + v \frac{\partial^2 u}{\partial x^2} - \frac{\partial (uv)}{\partial y} + v \frac{\partial^2 u}{\partial^2 y} - \frac{\partial p}{\partial x} + g_x \tag{4}$$

$$\frac{\partial v}{\partial t} = -\frac{\partial}{\partial x} \left(uv \right) + v \frac{\partial^2 v}{\partial x^2} - \frac{\partial \left(v^2 \right)}{\partial y} + v \frac{\partial^2 v}{\partial y^2} - \frac{\partial p}{\partial y} + gy \tag{5}$$

The governing equation can be solved by neglecting the pressure value first, using the fractional-step method. The following is the discretization of the governing equation for the droplet phenomenon.

2.2.1. Discretization of x and y directions

First order fractional-step formulation as follow,

$$\frac{\hat{u} - u^n}{\Delta t} = -L_x \left(\hat{u}^2 \right) + v.L_{xx} \left(\hat{u} \right) \tag{6}$$

$$\frac{\hat{v} - v^n}{\Delta t} = -L_x(\hat{u}\hat{v}) + v.L_{xx}(\hat{v}) \tag{7}$$

Second order fractional-step formulation as follow,

$$\frac{u^* - \hat{u}}{\Delta t} = -Ly\left(u^*v^*\right) + v\left(u^*\right) + g_{x} \tag{8}$$

$$\frac{v^* - \hat{v}}{\Delta t} = -Ly \left(v^* \frac{2}{v}\right) + v \left(v^*\right) + g_y \tag{9}$$

Where (\hat{u}, \hat{v}) are auxiliary components and operators L_x, L_{xx}, L_y, L_{yy} is defined as below,

$$L_{x}(\phi) = \frac{1}{\Delta x} \left(\Phi_{i+1/2, j} - \Phi_{i-1/2, j} \right)$$
 (10)

$$L_{v}(\phi) = \frac{1}{\Delta v} \left(\Phi_{i, j+1/2} - \Phi_{i, j-1/2} \right)$$
 (11)

$$L_{xx}(\phi) = \frac{1}{4\pi^2} \left(\Phi_{i+1, j} - 2\Phi_{i, j} - \Phi_{i-1, j} \right)$$
 (12)

$$L_{yy}(\phi) = \frac{1}{\Delta v^2} \left(\Phi_{i, j+1} - 2\Phi_{i, j} - \Phi_{i, j-1} \right)$$
 (13)

Where ϕ is general variable. To derive an efficient solution, the following linearization is required,

$$\hat{u}^2 = u^{n2} + 2u^n (\hat{u} - u^n) + 0(\Delta t^2)$$
 (14)

$$\hat{u}\hat{v} = u^{n}v^{n} + u^{n}(\hat{v} - v^{n}) + 0(\Delta t^{2})$$
 (15)

$$u^{*}v^{*} = \hat{u}\hat{v} + \hat{v}(u^{*} - \hat{u}) + 0(\Delta t^{2})$$
 (16)

$$u^{*2} = \hat{v}^2 + 2\hat{v}(v^* - \hat{v}) + 0(\Delta t^2) \tag{17}$$

Then linearize the above is substituted in to equations 6-9. Thus obtained the value of \hat{u} and \hat{v} from the equation of finite volume as follow,

$$\hat{u}_{i,j} + \Delta t. L_{x} \left(2u^{n}.\hat{u} \right)_{i,j} - v. \Delta t. L_{xx} \left(\hat{u}_{i,j} \right) = u_{i,j}^{n} + \Delta t. L_{x} \left(u^{n2} \right)_{i,j}$$
 (18)

and

$$\hat{v}_{i,j} + \Delta t. L_x \left(u^n . \hat{v} \right)_{i,j} - v. \Delta t. L_{xx} \left(\hat{v}_{i,j} \right) = v_{i,j}^n \tag{19}$$

These equations form a tridiagonal system often referred to as the tridiagonal matrix algorithm (TDMA) with the general concept as follows,

$$\begin{bmatrix} b_1 & c_1 & \cdots \\ a_2 & b_2 & c_2 \\ \vdots & \ddots & \ddots \end{bmatrix} \begin{bmatrix} \Phi_1 \\ \Phi_2 \\ \vdots \end{bmatrix} = \begin{bmatrix} RHS_1 \\ RHS_2 \\ \vdots \end{bmatrix}$$
 (20)

Where a_i, b_i, c_i are the main coefficients of the diagonal matrix, ϕ_1 and ϕ_2 are the variable of interest, RHS₁ and RHS₂ are the right-hand side coefficients whose values are already known. The form of the coefficients in equations (18) and (19) to be calculated using equation (20). The coefficient of equation (18) became as below,

$$a_{i} = -u_{l} \frac{\Delta t}{\Delta x} - S_{x}$$

$$b_{i} = 1 + \left(u_{r} - u_{l}\right) \frac{\Delta t}{\Delta x} + 2S_{x}$$

$$(21.a)$$

$$c_i = u_r \frac{\Delta t}{\Delta x} - S_x \tag{21.c}$$

$$\Phi_{i} = \hat{u}_{i,j}; \quad RHS_{i} = u_{i,j}^{n} + \frac{\Delta t}{\Delta s} \left(u_{r}^{2} - u_{l}^{2} \right)$$
 (22)

where,

$$u_r = \frac{1}{2} \left(u_{i+1, j}^n + u_{i, j}^n \right) \quad ; \quad u_l = \frac{1}{2} \left(u_{i, j}^n + u_{i-1, j}^n \right) \quad ; \quad S_x = \frac{v\Delta t}{\Delta x^2}$$
 (23)

For equation (19), the coefficient become as follow,

$$a_{i} = -\frac{1}{2}u_{l}\frac{\Delta t}{\Delta x} - S_{x} \quad ; \quad b_{i} = 1 + \frac{1}{2}\left(u_{r} - u_{l}\right)\frac{\Delta t}{\Delta x} + 2S_{x} \quad ; \quad c_{i} = \frac{1}{2}u_{l}\frac{\Delta t}{\Delta x} - S_{x}$$

$$\Phi_{i} = \hat{v}_{i, j}; \quad RHS_{i} = v_{i, j}^{n}$$

$$(24)$$

where,

$$u_r = \frac{1}{2} \left(u_{i,j+1}^n + u_{i,j}^n \right); u_l = \frac{1}{2} \left(u_{i-1,j}^n + u_{i-1,j}^n \right) (26)$$

Next step is determining the value of transient velocity u^* and v^* from equations (8) and (9) as follow,

$$u_{i,j}^{*} + \Delta t. L_{v} \left(\hat{v} u^{*} \right)_{i,j} - v. \Delta t. L_{vv} \left(u_{i,j}^{*} \right) = \hat{u}_{i,j} + \Delta t. g_{x}$$
 (27)

and

$$v_{i,j}^* + \Delta t \cdot Ly \left(2\hat{v}u^* \right)_{i,j} - v \cdot \Delta t \cdot L_{yy} \left(\hat{v}_{i,j}^* \right) = \hat{v}_{i,j}^* + \Delta t \cdot Ly \left(\hat{v}_{i,j}^2 \right) + \Delta t \cdot g_x \quad (28)$$

2.2.2. Pressure Correction

$$p_{i,j}^{\alpha+1} = \beta [A+B]^{-1} [C+D-E] + (1-\beta) p_{i,j}^{\alpha}$$
 (29)

$$A = \frac{1}{\Delta x^2} \left(\frac{1}{\rho_{i+1,j}^n + \rho_{i,j}^n} + \frac{1}{\rho_{i,j}^n + \rho_{i-1,j}^n} \right) \quad (29.a)$$

$$B = \frac{1}{\Delta y^2} \left(\frac{1}{\rho_{i,j+1}^n + \rho_{i,j}^n} + \frac{1}{\rho_{i,j}^n + \rho_{i,j-1}^n} \right) \quad (29.b)$$

$$C = \frac{1}{\Delta x^2} \left(\frac{p_{i+1,j}^{\alpha}}{\rho_{i+1,j}^{n} + \rho_{i,j}^{n}} + \frac{p_{i+1,j}^{\alpha+1}}{\rho_{i,j}^{n} + \rho_{i-1,j}^{n}} \right) \quad (29.c)$$

 $D = \frac{1}{\Delta y^{2}} \left(\frac{\rho_{i,j+1}^{\alpha}}{\rho_{i,j+1}^{n} + \rho_{i,j}^{n}} + \frac{\rho_{i,j-1}^{\alpha+1}}{\rho_{i,j}^{n} + \rho_{i,j-1}^{n}} \right) (29.d)$ $E = \frac{1}{2\Delta t} \left(\frac{u_{i+1/2,j}^{*} + u_{i-1/2,j}^{*}}{\Delta x} + \frac{v_{i,j+1/2}^{*} + v_{i,j-1/2}^{*}}{\Delta y} \right) (29.e)$

2.3. Computational Domain and Boundary Conditions

The computational domain is square box where the pressure control volume is placed inside the computational domain, so that the boundary of the pressure control volume at the edge of the domain coincides with the domain boundary. In the notation for a standard Staggered-grid Mesh, the pressure is assumed to be known at the center of the control volume outlined by a thick solid line. The horizontal velocity component (u) is torn off at the center of the left and right edges of this control volume and the vertical velocity component (v) is kept at the center of the top and bottom edges.

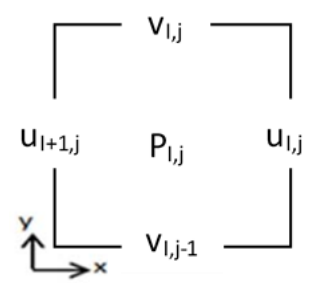


Figure 1. Computational domain in staggered-grid notation

To simplify the case, we must first determine the appropriate boundary conditions. As long as the center of the control volume coincides with the boundary conditions we can set the velocity in accordance with what it should be. For the rigid wall case, the normal velocity is usually zero and for the inflow boundary, the normal velocity is generally specified. The velocity equation at the boundary condition follows the following equation.

$$u_{wall} = (1/2)(u_{i,1} + u_{i,2})^{3}$$
 (30)

Where u_{wall} is the tangent velocity at the wall and $u_{i,1}$ is the shadow velocity. As long as the wall velocity and the velocity inside the domain $u_{i,2}$ are known, we can easily find the shadow velocity.

$$u_{i,1} = (1/2) (u_{wall} - u_{i,2})$$
 (31)

2.3. Numerical Code (MATLAB)

The implementation of the algorithm described above is written in the form of a script and run using MATLAB R2019 student version. The script is used to simulate the falling motion of a droplet that starts at the center of a square domain. As gravity accelerates the droplet's downward fall, the droplet becomes flatter and its outer part is pulled backward by the water flow.

3. Results and Discussion

This research is an advanced stage of what researchers have done in 2018. Referring to the article, it was found that the modeling developed by the researcher was consistent with that developed by Tryggvason (2012) [16]. The phenomenon of a single droplet hitting a solid surface is modeled in this study. The governing equations used in this modeling are the continuity equation, momentum equation for the case of unsteady flow and incompressible fluid and front-tracking equation to track the interface. The solution of the discretization of the governing equations in this study was carried out using the finite volume method implicit scheme. The focus of discussion in this study is to

determine the effect of variations in grid size and density ratio on the characteristics of the density field.

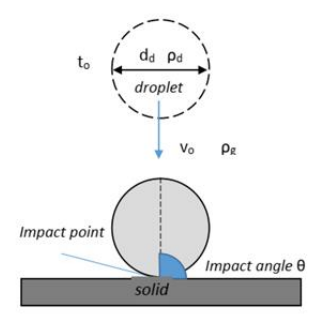


Figure 2. Droplet impacting solid surface illustration

A single droplet of liquid falling in the air vertically with a uniform velocity impacting a horizontal surface at room temperature is shown in Fig 2. The diameter of the droplet in free fall before impacting the surface is $d_d = 0.2$ cm. The impact angle when the droplet impacts the surface is $\theta = 90^{\circ}$. Variations of modeling conditions are shown in table 1. Validation of the modeling results is done by comparing the velocity field displayed in 2D images to the modeling done by Tryggvason 2012 with an explicit scheme. The density field is the focus of this study and is shown for each case in Table 1 below,

Table 1. Variations of single droplet modeling.

Table 1. Variations of single droplet modeling.		
Cases	Interface	Surface Tension
1	not tracked	neglected
2	tracked	neglected
3	tracked	not neglected

The three variations above are given the grid size, density ratio (ρ_d/ρ_g) and time step (Δt) respectively: grid size by 32, density ratio by 2 and (Δt) by 0.00125 s.

3.1. Validation of Single Droplet Modelling

The validation of this research is done by comparing the modeling results with the numerical results developed by Tryggvason 2012. These two modelings have different schemes in discretizing the governing equations where an implicit scheme is performed in this modeling and Tryggvason developed modeling with an explicit scheme.

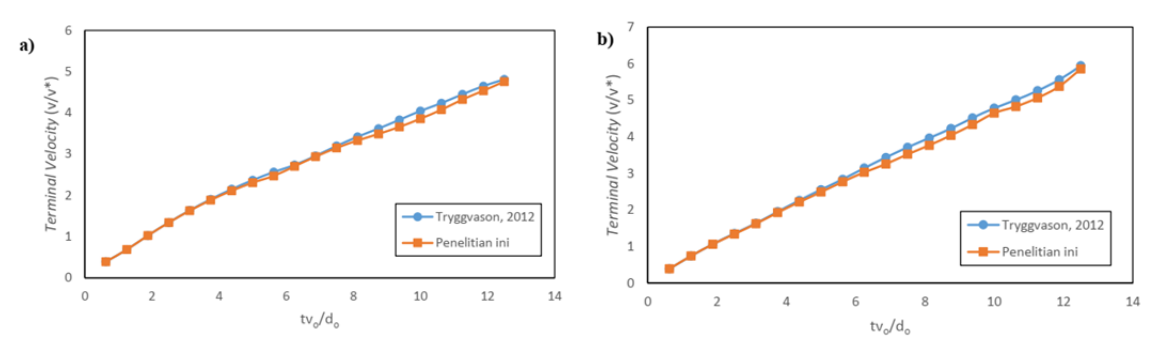


Figure 3. Terminal velocity (v/v^*) as dimensionless function (tv_0/d_0) , a) case 1 and b) case 2

The non-dimensional velocity change as a function of time $t^*(tv_0/d_d)$ is shown in Fig 3. The non-dimensional velocity is represented by the terminal velocity (v/v^*) where the actual velocity v is divided by the reference velocity v. The reference velocity is obtained from the equation $v^* = (\rho_d - \rho_0) g_d^2/\mu$. The notation ρ_0 represents the density value around the droplet (surrounding fluid). As can

be seen from Fig 3, the change in velocity as a function of time for the first and second cases in this study has the same value trend as that done by Tryggvason (2012) [16].

3.2 Characteristic of Density Field

Density field is the distribution of density values indicated by a density jump between the two fluids. As long as there is no temperature influence in the computational process, the density value of the droplet must have a uniform value. The density field in this modeling can be seen in Figures 4 and 5 below,

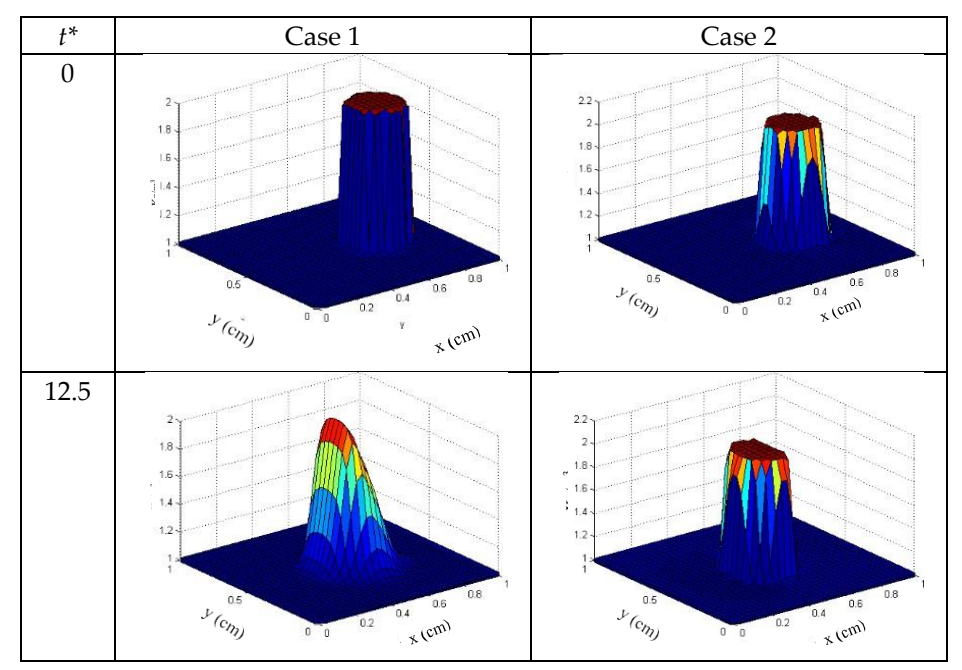


Figure 4. Initial and on-start density fields, case 1 and 2

Modeling in the first case, the interface is not defined while for the second case the interface is defined by the front-tracking method. The density spike does not occur at t^* =12.5 for the first case so that the phase in the computational domain is difficult to distinguish between the droplet and the surrounding fluid. This modeling produces results that do not match the actual phenomenon. As long as the interface separating the contacting fluids is not defined, the modeling results obtained do not match the physical phenomenon. In the second case, a spike in density value is marked by a marker point and the separation interface between the droplet and the surrounding fluid is reconstructed. The interface is tracked using the front-tracking method based on the location of the density jump.

Figure 5 shows the density fields for the second and third cases. The interface for each case is tracked by front-tracking method with surface tension variation. In the second case surface tension is ignored in modeling the droplet phenomenon while for the third case the modeling involves surface tension in solving the governing equations. When t^* at the position (0 - 12.5) of free falling droplet, there is no significant difference in the density field for each case. However, after the droplet hits the horizontal surface, there is a difference in the second and third cases. The condition of the density field.

The condition of the density field before the droplet hits the surface occurs at t^* = 25 and after hitting the surface occurs at t^* = 32.5. As can be seen from Figure 5, the density field has an irregular shape before and after the droplet hits the surface. This is because the discretization solution of this case does not involve surface tension, so the shape of the droplet cannot be maintained when it hits a surface.

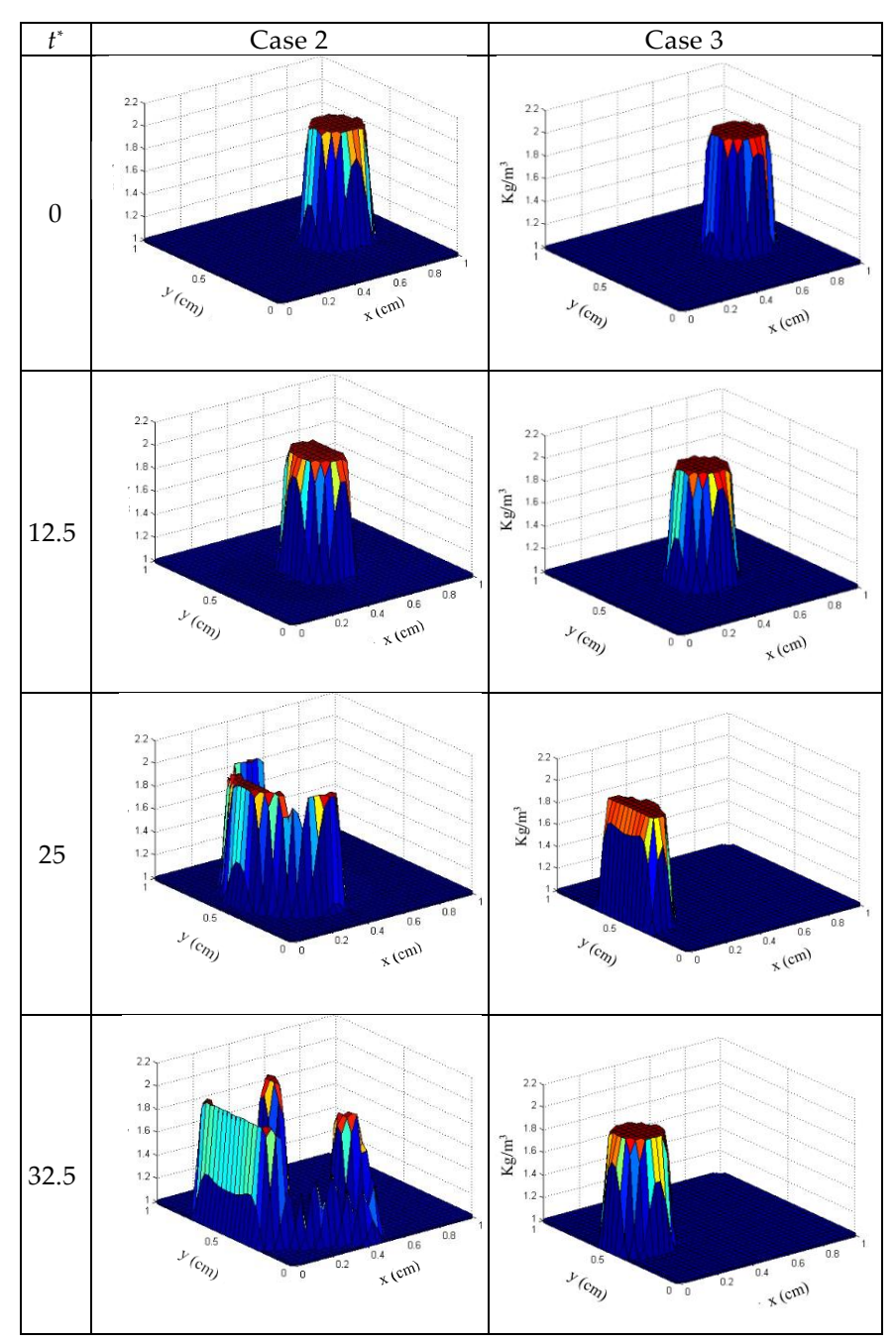


Figure 5. Initial and on-start density fields, case 2 and 3

In contrast to the modeling in the third case, when surface tension is taken into account in the completion of discretization, several phenomena occur when droplets hit the surface as shown in Figures 5 and 6. These phenomena are spreading, recoiling and bouncing up. When $t^* = 25$ droplets hit the surface and the phenomenon of spreading occurs. The condition of the droplet after impacting is shown in Figure 5 at $t^* = 32.5$. At this stage the phenomenon of bouncing up occurs. This spike in density value indicates a phase difference between the two fluids.

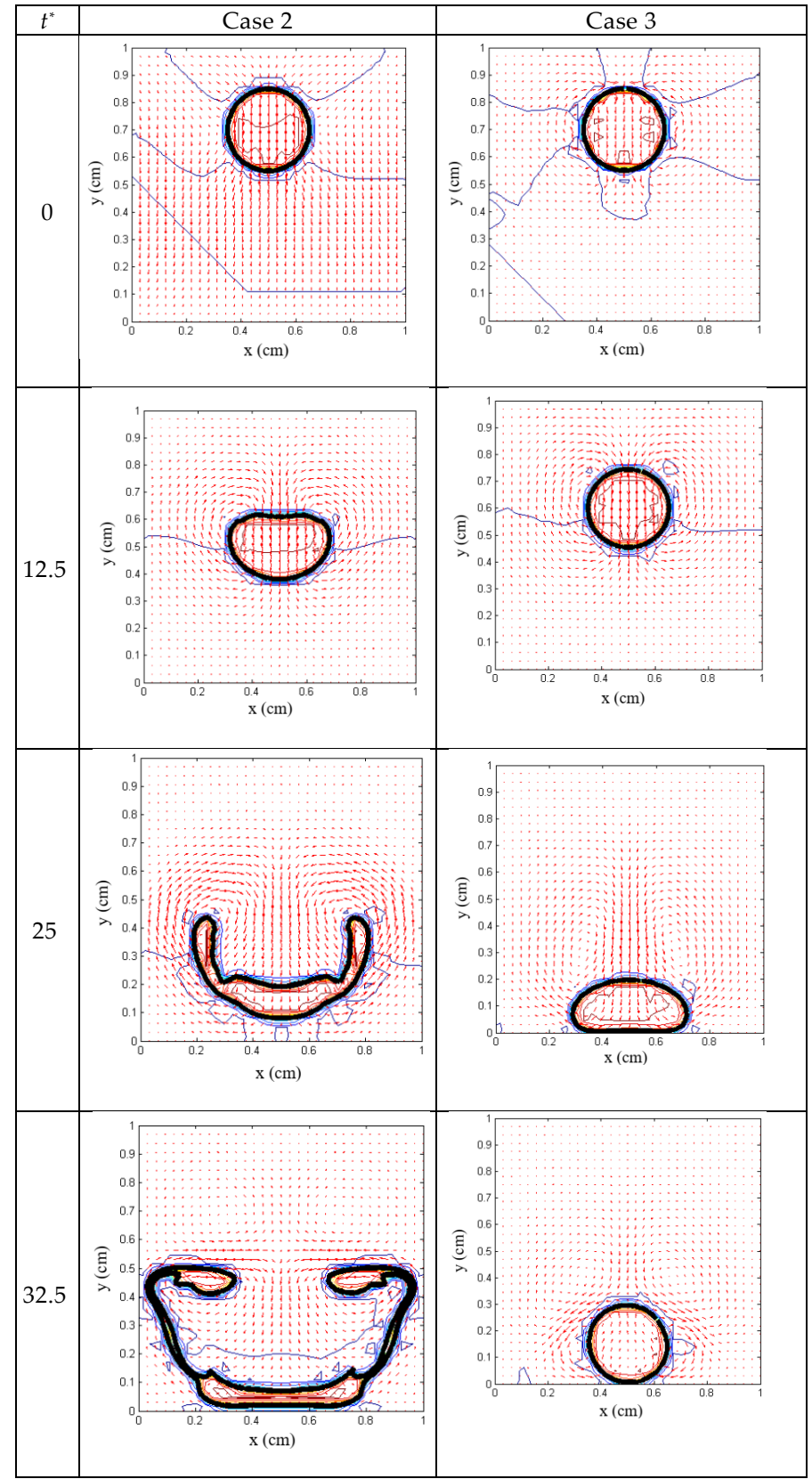


Figure 6. Velocity fields 2D visualization, case 2 and 3

The density jump portrait of the front-tracking method is affected by the grid size using a 2D view. Figure 7 shows the density jump portraits in this study, (a) the density field with the expected density jump, (b) grid size 162, (c) grid size 322 and (d) grid size 642. The 642 resolution grid displays a steeper density jump and is closer to the exact solution condition (a) than the 162 and 322 grid sizes. The smaller the grid size (the greater the number of grids), the more accurate the results but the more complicated and time-consuming the calculation.

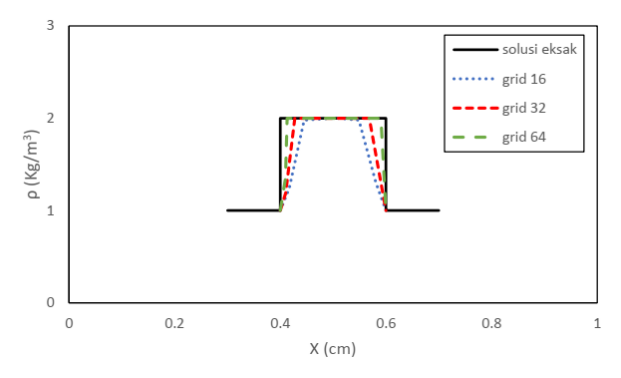


Figure 7. Density jumps, exact solution, grid size 16², 32², 64².

4. Conclusions

Modeling of droplets impacting and spreading on a horizontal surface is performed using the finite volume method - front tracking with an implicit scheme. To validate this modeling is conducted by comparing with the model that has been developed by Tryygvason 2012 [16] using the finite volume method - front tracking explicit scheme. Changes in non-dimensional velocity as a function of time $t^*(tvo/dd)$ and non-dimensional velocity represented by terminal velocity (v/v^*) are plotted so that this modeling is found to be in accordance with the model developed by Tryggvason 2012. In this study, the variables used are the case variation using interface tracking and surface tension with constant density ratio. The density field characteristic of the multi-phase phenomenon is shown by the density jump. The interface is tracked using the front-tracking method based on the location of the density jump. Surface tension influences the shape of the droplet before and after hitting the surface, resulting in spreading, recoiling and bouncing up phenomena. In addition, the grid size is known to have an influence on this modeling. The smaller the grid size (the greater the number of grids), the more accurate the density jump obtained and the closer to the actual result.

Acknowledgments

The authors are very grateful to the Department of Mechanical, Faculty of Engineering, University of Lampung for supporting this research.

References

- [1] Y. Ren, J. Cai, and H. Pitsch, "Theoretical single-droplet model for particle formation in flame spray pyrolysis," *Energy & Fuels*, vol. 35, no. 2, pp. 1750–1759, 2021.
- [2] A. Aboubakri, C. Yanik, Y. Akkuş, A. Koşar, and A. K. Sadaghiani, "Numerical and experimental investigation on evaporation of water droplet on surfaces with mixed wettability," in *International Conference on Nanochannels, Microchannels, and Minichannels*, American Society of Mechanical Engineers, 2020, p. V001T06A002.
- [3] S. Mehdi, L. Yangpeng, C. Hadrien, L. Fabrice, W. Xishi, and C. Guillaume, "Fluorescence lifetime

- measurements applied to the characterization of the droplet temperature in sprays," *Exp. Fluids*, vol. 62, pp. 1–19, 2021.
- [4] S. Basu, A. K. Agarwal, A. Mukhopadhyay, and C. Patel, "Introduction to droplets and sprays: Applications for combustion and propulsion," *Droplets Sprays Appl. Combust. Propuls.*, pp. 3–6, 2018.
- [5] S. Sahu, "Analysis of droplet clustering in air-assist sprays using Voronoi tessellations," *Phys. Fluids*, vol. 30, no. 12, 2018.
- [6] V. Parihar, S. Chakraborty, S. Das, S. Chakraborty, and S. DasGupta, "Role of anisotropic pinning and liquid properties during partial rebound of droplets on unidirectionally structured hydrophobic surfaces," *Chem. Eng. Sci.*, vol. 230, p. 116197, 2021.
- [7] M. Nasiri, G. Amini, C. Moreau, and A. Dolatabadi, "Hollow droplet impact on a solid surface," *Int. J. Multiph. Flow*, vol. 143, p. 103740, 2021.
- [8] X. Fan and X. Lu, "Numerical simulation of single droplet combustion characteristics in high temperature convection environment," in *IOP Conference Series: Earth and Environmental Science*, IOP Publishing, 2019, p. 62050.
- [9] D. Kurniawan, E. Budiana, D. Deendarlianto, and I. Indarto, "Simulasi Numerik Fenomena Single Droplet Menggunakan Metode Volume Hingga dan Front-Tracking," *POROS*, vol. 15, no. 2, pp. 84–91, 2017.
- [10] E. Mawarsih, E. P. Budiana, Deendarlianto, Indarto, and S. Kamal, "Numerical simulation of single droplet phenomenon using method finite difference and front-tracking," AIP Conf. Proc., vol. 2296, no. January 2019, 2020, doi: 10.1063/5.0030454.
- [11] Y. Takata *et al.*, "The interfacial dynamics of the micrometric droplet diameters during the impacting onto inclined hot surfaces," *Int. J. Heat Mass Transf.*, vol. 126, pp. 39–51, 2018.
- [12] P. Boggavarapu, R. V Ravikrishna, and M. M. Avulapati, "Droplet Combustion Behavior and Spray Characteristics of Diesel–Ethanol–Jatropha Oil Ternary Fuel Blends Under High-Pressure Evaporating Conditions," J. Energy Resour. Technol., vol. 146, p. 32301, 2024.
- [13] Deendarlianto *et al.*, "Effect of static contact angle on the droplet dynamics during the evaporation of a water droplet on the hot walls," *Int. J. Heat Mass Transf.*, vol. 71, pp. 691–705, 2014, doi: 10.1016/j.ijheatmasstransfer.2013.12.066.
- [14] E. Kumolosari, A. Sandi, Y. V. Yoanita, S. T. Pinindriya, and D. Kurniawan, "SIMULASI PERFORMA AERODINAMIKA NACA 1408 PADA APLIKASI TURBIN ANGIN DENGAN VARIASI PANJANG GURNEY FLAP," *MUSTEK ANIM HA*, vol. 12, no. 02, pp. 96–101, 2023.
- [15] C. M. Lemos, "FDFLOW: a FORTRAN-77 solver for 2-D incompressible fluid flow," *Comput. Geosci.*, vol. 20, no. 3, pp. 265–291, 1994.
- [16] G. Tryggvason, "A Front-tracking/Finite-Volume Navier-Stokes Solver for Direct Numerical Simulations of Multiphase Flows," 2012.



This is an open access publication under the terms and conditions of the Creative Commons Attribution (CC BY) license (http://creativecommons.org/licenses/by/4.0/).